

# Parity violation in radiative emission of neutrino pair from metastable states of heavy alkaline earth atoms

M. Yoshimura, N. Sasao<sup>†</sup>, and S. Uetake

Center of Quantum Universe, Faculty of Science, Okayama University  
Tsushima-naka 3-1-1 Kita-ku Okayama 700-8530 Japan

<sup>†</sup> Research Core for Extreme Quantum World, Okayama University  
Tsushima-naka 3-1-1 Kita-ku Okayama 700-8530 Japan

## ABSTRACT

Macro-coherent atomic de-excitation involving a neutrino pair emission, radiative emission of neutrino pair (RENP)  $|e\rangle \rightarrow |g\rangle + \gamma + \nu_i \nu_j$  (with  $\gamma$  a photon and  $\nu_i$  a neutrino mass eigenstate), is a new experimental tool to determine undetermined neutrino parameters such as the smallest neutrino mass and distinction of Majorana and Dirac neutrinos. The best way to prove that the atomic RENP process accompanied by unseen neutrino pair involves weak interaction is to measure parity violating (PV) quantities. We quantitatively study how this is achieved. The basic mechanism of how a favorable situation for PV may arise from the fundamental electroweak theory (extended to incorporate finite neutrino masses) is emphasized and calculation of dependence of PV observables on applied magnetic field is worked out for heavy target atoms of alkaline earth like level structure such as Sr, Yb, Hg, Xe. Numerically calculated parity violating rates and asymmetry are presented for Yb  $J = 2 \rightarrow 0$  and  $J = 0 \rightarrow 0$  RENP.

Key words

Neutrino mass, Parity violation, Majorana particle, Beyond the standard gauge theory

## I Introduction

In remarkable achievements neutrino oscillation experiments have succeeded in determining five elements of the neutrino mass matrix [1]; three mixing angles and two mass squared differences. They however left undetermined important parameters, possibly three parameters in the Majorana neutrino case; the absolute neutrino mass (or the smallest neutrino mass) scale and the two Majorana CP phases. Conventional targets in ongoing experiments of exploring a part of these undetermined neutrino parameters have been nuclei. Direct measurement of the end point spectrum of beta decay such as tritium [2] and (neutrino-less) double beta decay [3] are two main methods to resolve these outstanding problems. One serious problem of nuclear target experiments is the remoteness of released nuclear energies from the expected small neutrino mass of a fraction of eV.

In a series of theoretical papers we proposed and elaborated a new, systematic experimental method to probe the neutrino mass matrix using macro-coherent atomic process, namely radiative emission of neutrino pair (RENP),  $|e\rangle \rightarrow |g\rangle + \gamma + \nu\nu$  [4], [5]. We discussed how to enhance otherwise small neutrino pair emission rates [6], [5], and how to extract neutrino parameters from the photon energy spectrum [7]. In the most recent work we pointed out how to obtain a much larger RENP rate [8] using a coherent neutrino pair emission from the zero-th component of vector current much like the enhanced admixture of different parity states in heavy atoms [9] for atomic parity violation experiments [10], [11], [12]. Our experimental efforts towards RENP are briefly described in [5].

Parity violation (PV) is one of the most important features that characterizes weak interaction distinguishing from other interactions. This feature is automatically built in the standard electroweak theory as a preference of handedness or chirality of neutrino, describing neutrinos by two component spinors unlike all other charged leptons and quarks of four components. It has been the key feature to prove the nature of weak processes since the classic work of Lee and Yang. In particular, parity violation in electron interaction with nuclei caused by Z-boson exchange has been discovered in electron scattering and atomic parity violation experiments, thereby establishing the electroweak unification.

In the present work we examine how parity violation in our proposed process of RENP may arise from the fundamental electroweak theory. If parity violating effects turn out to be large, it should help to experimentally identify RENP and prove that weak interaction is involved in the process. It would be the best way to reject QED backgrounds in RENP experiments. A large parity violating (PV) observable and asymmetry is expected in the case of de-excitation between states of different parities, and we shall work out RENP rates for alkaline earth like atoms, examples being (1)  $(6s6p)^3P_2$  orbital state at  $\sim 2.44\text{eV}$  of neutral Yb, (2)  $^3P_0$  state slightly below this level, and similar ones for Sr, Hg and Xe, all having low lying excited states made of  $ns, n'p$  or rare earth atoms of electron-hole pair of the same quantum numbers.

The rest of this work is organized as follows. In Section II how PV observables in RENP process may arise in the standard electroweak theory (with finite neutrino masses) by listing all terms of neutrino interaction with electrons and quarks to the leading and next leading orders of  $1/\text{mass}$ . Some technical details on the phase space integral of neutrino pair variables (helicities and momenta) that have a direct relevance to emergence of parity odd quantities are relegated to Appendix B. It is found that without external electric field transitions between different parity states are required for large PV effects. In Section III we show that the best target atoms are alkaline atoms of two-electron system which have two metastable states of  $^3P_2, ^3P_0$ . To produce large PV effects it is important to use heavy atoms where  $LS$  coupling scheme breaks down, requiring calculations in the intermediate coupling scheme.. Some aspects of the intermediate coupling scheme for heavy atoms are explained in Appendix C. In Section IV basic diagrams and corresponding perturbation amplitudes are identified. Importance of hyperfine interaction is stressed. We then calculate in Section V amplitudes of RENP, emphasizing how the magnetic field dependence is disentangled. In Section VI RENP rates, both parity conserving (PC) and PV, are calculated. We then illustrate results of numerical computations on PV observables; PV asymmetry under field and circular polarization reversal, taking the example of the Yb  $J = 2 \rightarrow 0$  transition. The section VII is devoted to Yb  $J = 0 \rightarrow 0$  RENP. The rest consists of summary and Appendices which collect important technical details not fully explained in the

main text..

We shall calculate amplitudes using perturbation theory in non-relativistic quantum mechanics, hence the time ordering in higher orders of perturbation should be treated with care.

Throughout this work we use the natural unit of  $\hbar = c = 1$ .

## II How parity odd observables arise in RENP

Typical RENP experiments use four lasers for trigger and excitation. For instance, two continuous wave (CW) lasers of different frequencies,  $\omega_i, \omega_1 + \omega_2 = \epsilon_{eg}$  with  $\epsilon_{eg}$  the energy difference between the initial  $|e\rangle$  state and the final  $|g\rangle$  state, are used as triggers in counter propagating directions (taken along z-axis), while two excitation lasers of Raman type of frequencies,  $\epsilon_p, \omega_s$  with  $\epsilon_p - \omega_s = \epsilon_{eg}$  are irradiated in pulses. Measured variables at the time of excitation pulse irradiation are the number of events at each trigger frequency  $\omega$ . By repeating measurements at different trigger frequency combinations, one obtains the photon energy spectrum at different frequency  $\omega = \omega_1 (< \omega_2)$  accompanying the neutrino pair.

The macro-coherent three-body RENP process  $|e\rangle \rightarrow |g\rangle + \gamma + \nu\nu$  conserves both the energy and the momentum [5], giving continuous photon energy spectrum with thresholds. Note that the spontaneous decay of dipole transition from atoms conserves the energy alone, hence their spectrum is continuous despite of a single particle decay. In RENP there are six photon energy thresholds at  $\omega_{ij} = \epsilon_{eg}/2 - (m_i + m_j)^2/2\epsilon_{eg}$  where  $m_{i(j)}, i, j = 1, 2, 3$  is neutrino mass of eigenstate. Decomposition into six different threshold regions is made possible by excellent energy resolution of trigger laser frequencies.

Measurement of the photon energy spectrum is regarded as a parity even observable and arises from parity conserving parts of basic interaction of the weak process. The only handle for this experiment is the frequency of trigger lasers, whose accuracy of  $10^{-15}$  is readily obtained with a rapid development of laser technologies [13]. However, there are many other experimental handles in atomic experiments, giving rise to measurements of PV quantities with relative easiness.

Identification of parity violating (PV) quantities in RENP under the circumstance of accompanying unseen neutrino pair is a non-trivial problem, and we shall describe our method of how identification of PV effects and search for candidate atoms is made in general terms first, postponing the choice of target states later.

PV effects arise from interference of two RENP amplitudes of parity even (PE) and parity odd (PO). Note that the rate arising from the squared PO and the squared PE amplitudes give PC rates. Extracting explicitly neutrino pair emission vertex, interference term may arise in three ways: the first way via interference between one term in  $A_0\nu_1^\dagger\nu_2$ , and the other in  $\vec{A} \cdot \nu_1^\dagger\vec{\sigma}\nu_2$ , and the second and the third ways between two decomposed terms either in  $A_0^i$  or  $\vec{A}^i, i = 1, 2, \dots$ . Each of  $A_\alpha^i, \alpha = 0, 1, 2, 3$  contains product of atomic matrix elements, couplings and energy denominators in perturbation theory. We use two component notation for electron operators in  $A_\alpha$ , following the  $\gamma_5$ -diagonal representation of [4]. Relevant leading terms for PO and PE terms are taken from Appendix A: written in terms of the electron field operator in the non-relativistic limit of  $\gamma_5$ -diagonal representation, they are

$$A_0 \propto e^\dagger \left( b_{12} + \delta_{12} 2 \sin^2 \theta_w \vec{\sigma} \cdot \frac{\vec{p}}{m_e} + O\left(\frac{1}{m_e^2}\right) \right) e + \delta_{12} j_q^0, \quad j_q^0 = -\frac{1}{2} j_n^0 + \frac{1}{2} (1 - 4 \sin^2 \theta_w) j_p^0, \quad (1)$$

$$\vec{A} \propto e^\dagger \left( a_{12} \vec{\sigma} + \delta_{12} 2 \sin^2 \theta_w \frac{1}{m_e} (\vec{p} - i \vec{\sigma} \times \vec{p}) + O\left(\frac{1}{m_e^2}\right) \right) e, \quad (2)$$

where couplings  $a_{12}, b_{12}$  are of order unity and written in terms of the neutrino mixing angles.  $m_e$  is the electron mass. Their explicit forms are given in equations of Appendix A. The term  $j_q^0$  is the nuclear mono-pole current contribution which gives rise to coherently added constituent numbers [8]. We disregarded terms of orders of  $1/m_e^2$  and  $1/m_N$  ( $1/\text{nucleon mass}$ ),

In order to calculate rates, both parity conserving (PC) and parity violating (PV), added amplitudes are squared, and one proceeds to calculate summation over neutrino helicities and momenta, since neutrino variables are impossible to measure under usual circumstances. Thus, one deals with a phase space integral

of neutrino pair momenta after helicity summation in the form,

$$\int d\mathcal{P}_\nu \sum_{h_i} |A_0 \nu_1^\dagger \nu_2 + \vec{A} \cdot \nu_1^\dagger \vec{\sigma} \nu_2|^2, \quad d\mathcal{P}_\nu = \frac{d^3 p_1 d^3 p_2}{(2\pi)^2} \delta(\omega + E_1 + E_2 - \epsilon_{eg}) \delta(\vec{k} + \vec{p}_1 + \vec{p}_2). \quad (3)$$

All necessary phase space integrals are listed in Appendix B. The non-trivial part of the phase space integral relevant to PV interference arises from the term  $-2\Re(A_0 \vec{A}^*)$  multiplied by

$$\int d\mathcal{P}_\nu \left( \frac{\vec{p}_1}{E_1} + \frac{\vec{p}_2}{E_2} \right) = \vec{k} \frac{J_{12}(\omega)}{\omega}, \quad (4)$$

where  $J_{12}(\omega)$  is a scalar function given in Appendix B. The photon momentum vector  $\vec{k}$  is thus multiplied to  $-2\Re(A_0 \vec{A}^*)$ , which give three types of electron operators proportional to

$$\vec{k} \cdot \vec{\sigma}, \quad \frac{\vec{k} \cdot \vec{p}}{m_e}, \quad i \frac{\vec{k} \cdot \vec{\sigma} \times \vec{p}}{m_e}. \quad (5)$$

All of these are hermitian. The only PO operator is the first one,  $\vec{k} \cdot \vec{\sigma}$ . The remaining amplitude multiplied to this involves PC QED interaction such as  $\vec{d} \cdot \vec{E}$ , hence this term alone can be adopted for PO amplitude.

The fact that PV term arises without the suppression of  $1/m_e$  might appear surprising. This conclusion is consistent with the ordinary view that PV effects must arise from interference of parity odd combination of  $V \cdot A$ . The spin current of electron  $\propto \vec{\sigma}$  arises from spatial component of 4-axial vector  $\propto \gamma^\alpha \gamma_5$  in the non-relativistic limit, while the nuclear mono-pole current  $\propto j_q^0$  arises from time component of 4-vector current  $\propto \gamma_\alpha$ . It is the unique combination of electron and nuclear current operators that gives rise to large PV terms without the suppression of  $1/m_e$  order, which became possible only with the advent of nuclear mono-pole contribution given in [8]. This excludes the other two possibilities of having  $1/m_e$  suppression for PV effect. We refer to Appendix A on technical aspects of PO operators.

### III Basic mechanism in heavy alkaline earth atoms

We shall first examine consequences of the conclusion of the previous section that RENP transition for a large PV measurement involves states of different parities in the initial and the final states. The simplest possibility might be use of the lowest excited state of alkali atoms taken as the initial  $|e\rangle$  state. The RENP of alkali atom however must compete with a fast E1 transition, and it may be experimentally difficult to measure PV quantity under a large signal to the background ratio. We shall not consider this possibility any further.

The next easiest may be two-electron system consisting of angular momentum combination of parity odd  $sp$  (two-electron system of the orbital angular momentum  $l = 0$  and 1). This combination appears as the first excited group of levels in alkaline earth atoms. Two electrons may be either in the spin triplet or the spin singlet state in the terminology of the  $LS$  coupling scheme. Thus, one has four different states (with the usual magnetic degeneracy of energies),  $^3P_2, ^3P_1, ^3P_0, ^1P_1$ , the atomic term symbol of  $^{2S+1}L_J$  being used [14].

Another important consideration is that it is better to use heavy (large atomic number) atoms for large RENP rates [8]. This poses a problem of state mixing in the  $LS$  scheme, which requires the use of intermediate coupling scheme [15]. The  $LS$  coupling scheme is based on the assumption that electrostatic interaction between electrons is much larger than the spin-orbit interaction  $\sum_i \xi(r_i) \vec{l}_i \cdot \vec{s}_i$ . In heavy atoms such as Pb, however, the spin-orbit interaction becomes larger and the  $jj$  coupling scheme becomes a better description [15]. Nevertheless most of heavy atoms is well described by the intermediate coupling scheme using the  $LS$  basis.

In the intermediate coupling scheme applied to heavy alkaline earth atoms, one considers the mixing among states of the same total angular momentum. This is because the total angular momentum is conserved

under the presence of the spin-orbit interaction. This type of mixing occurs for  $^3P_1$  and  $^1P_1$  of the  $LS$  scheme. Energy eigenstates are given in terms of the  $LS$  basis,

$$|^+P_1\rangle = \cos\theta|^1P_1\rangle + \sin\theta|^3P_1\rangle, \quad |^-P_1\rangle = \cos\theta|^3P_1\rangle - \sin\theta|^1P_1\rangle, \quad (6)$$

(with  $\pm$  denoting larger/smaller energy state) where the angle  $\theta$  is determined by the strength of spin-orbit interaction in the system and is related to experimental data of level energies. In the Yb case  $\sin\theta \sim 0.16$ , as shown in Appendix D, where some further details of the intermediate coupling scheme are also described. A relatively large dipole moments  $d(|^-P_1\rangle \rightarrow |^1S_0\rangle)$  needed for sizable RENP is induced by a non-vanishing value of  $\theta$ .

We shall consider  $^3P_2$  de-excitation for RENP. The  $^3P_0$  case is treated separately in Section VII. Due to the quantum number changes both in the orbital and the spin parts one needs at least two virtual transitions for de-excitation of  $^3P_2 \rightarrow ^1S_0$ . Relevant PE and PO diagrams leading to large amplitudes are depicted in Fig(1). PO diagram involves valence electron alone and contains matrix elements of the spin current of neutrino pair emission and E1 photon emission. PE diagram contains a large nuclear mono-pole current assisted by hyperfine interaction, which causes the necessary quantum number change to valence electron.

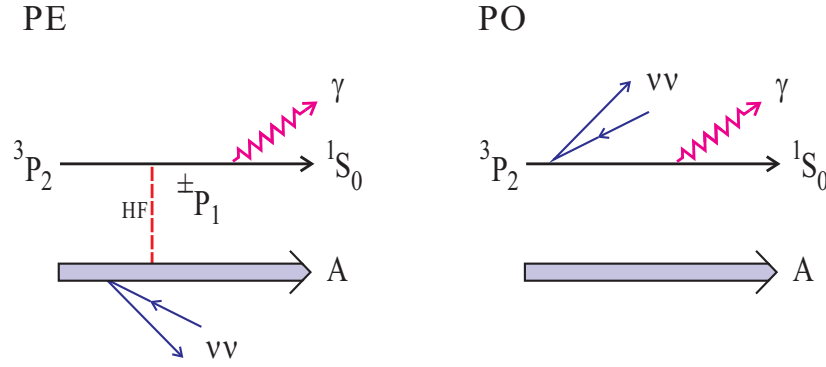


Figure 1: Parity even (PE) and odd (PO) diagram contributions. HF given by dashed line is hyperfine mixing interaction as described in the text.

Hyperfine interaction is caused by the nuclear magnetic field and quadrupole field. For simplicity we shall consider the magnetic hyperfine interaction alone by taking the nuclear spin of  $I = 1/2$  which excludes the possibility of quadrupole interaction [16]. Both Yb and Xe have isotopes of large natural abundances of this spin magnitude. The magnetic hyperfine interaction consists of dipole-dipole interaction and Fermi contact interaction,

$$\mathcal{H}_h = \vec{I} \cdot \vec{A}, \quad \vec{A} = g_e g_N \mu_B \mu_N \left( \sum_i \frac{\vec{l}_i - \vec{s}_i}{r_i^3} + \frac{3\vec{r}_i \vec{s}_i \cdot \vec{r}_i}{r_i^5} + \frac{8\pi}{3} \delta(\vec{r}) \vec{s}_i \right). \quad (7)$$

In the alkaline earth atom both of these contribute, the p-electron participating in the dipole-dipole interaction while the s-electron in the Fermi interaction. Matrix elements of this interaction are given in Appendix.

The main effect of hyperfine interaction in the PE amplitude is to give rise to non-vanishing vertex between  $^3P_1$  component in the levels  $^{\pm}P_1$  and  $^3P_2$ , which is given by

$$\langle ^1S | \vec{d} \cdot \vec{E} | ^{\pm}P_1 \rangle \langle ^{\pm}P_1 | \mathcal{H}_h | ^3P_2 \rangle. \quad (8)$$

Mixing caused by hyperfine interaction gives non-vanishing off-diagonal matrix elements for  $F = 3/2$  states,

$$\langle ^-P_{13/2} | \vec{I} \cdot \vec{A} | ^3P_{23/2} \rangle = \frac{\sqrt{5}}{8} (b - \frac{6}{5}a) \cos \theta + \frac{1}{4} \sqrt{\frac{5}{2}} (b - \frac{8}{5}a) \sin \theta, \quad (9)$$

$$\langle ^+P_{13/2} | \vec{I} \cdot \vec{A} | ^3P_{23/2} \rangle = -\frac{1}{4} \sqrt{\frac{5}{2}} (b - \frac{8}{5}a) \cos \theta + \frac{\sqrt{5}}{8} (b - \frac{6}{5}a) \sin \theta, \quad (10)$$

$$a = g_e g_N \mu_B \mu_N \langle 6p | \frac{1}{r^3} | 6p \rangle, \quad b = g_e g_N \mu_B \mu_N \frac{8\pi}{3} |\psi_{6s}(0)|^2. \quad (11)$$

Hyperfine parameters  $b, a$  may be determined by experimental data of hyperfine splitting of  $^3P_2, ^\pm P_1$ , as discussed in Appendix. The dominant parameter for Yb is  $b \sim 13\text{GHz}$  and the mixing amplitude is of order  $\sqrt{5}b \cos \theta / 8 \sim 3.5\text{GHz} \sim 2.3\mu\text{eV}$ .

#### IV Magnetic factors and PV observables

We consider application of external magnetic field to orient atoms which makes easier to produce various types of PV observables. The simplest among these is a PO angular distribution of emitted photon from polarized atom. The magnetic field is applied, for generality, to a tilted direction from the trigger axis (defined by z-axis) by an angle  $\theta_m$ . All projected angular momenta are taken along the magnetic field direction. Hence the angular part is described by

$$|J, \tilde{M}\rangle = e^{-i\theta_m J_y} |J, M\rangle = \sum_{M'} d_{M, M'}^J(\theta_m) |J, M'\rangle, \quad (12)$$

where  $d_{M, M'}^J(\theta_m)$  is the Wigner d-function or the rotation matrix in the terminology of [17]. Furthermore, two types of circular polarization, R and L or  $h = \pm 1$ , for trigger (hence RENP emitted) photon are considered. Amplitudes and rates are thus functions of  $\theta_m$  and  $h$ . Helicity dependence is readily worked out by taking the E1 dipole element proportional to components of spherical harmonics  $Y_{1, \pm 1}$ .

Components of magnetic factors are defined by various matrix elements sandwiched between these tilted states. For instance, E1 emission is given by matrix elements of

$$\begin{aligned} d\langle J, \tilde{M} | Y_{1, \pm 1} | J', \tilde{M}' \rangle &= d \sum_{M_1, M_2} d_{M, M_1}^J d_{M', M_2}^{J'} \langle J, M_1 | Y_{1, \pm 1} | J', M_2 \rangle \\ &= d \sum_{M_2} d_{M, M_2 \pm 1}^J d_{M', M_2}^{J'} \langle J, M_2 \pm 1 | Y_{1, \pm 1} | J', M_2 \rangle, \end{aligned} \quad (13)$$

RENP rates are functions of the angle  $\theta_m$  and circular polarization  $h = \pm$  of the trigger field. Two readily calculable PV asymmetries are rate differences under the magnetic field reversal and under the polarization reversal. We call these two asymmetries as PV asymmetry under field reversal and symmetry under polarization reversal.

For definiteness let us consider RENP transition from  $^3P_2, F = 3/2$  where  $\vec{F}$  is the angular momentum sum of electrons and nucleus. Magnetic angular factors we need for PV rate differences are

$$\mathcal{M}_B(x) = -\sqrt{3} \cos^3 x, \quad \mathcal{M}_h(x) = \frac{\sqrt{3}}{4} (1 + 3 \cos(2x)), \quad (14)$$

and for PC quantities

$$(1) \mathcal{M}_{\text{PC1}}(x) = \frac{1}{4} (3 + \cos(2x)), \quad (15)$$

$$(2) \mathcal{M}_{\text{PC2}}(x) = \frac{3}{4} (2 + \cos(2x) + \cos(4x)). \quad (16)$$

PV asymmetry  $\mathcal{M}_B$  is related to the one under field reversal, while  $\mathcal{M}_h(x)$  to the one under polarization reversal. These functions are derived from combinations of Wigner d-functions in Appendix. In PV asymmetry under field reversal one needs the difference in two directions,  $x$  and  $\pi - x$ ;  $\mathcal{M}_B(x) - \mathcal{M}_B(\pi - x) \neq 0$ . The simplest PV asymmetry of this kind is the forward-backward asymmetry for  $x = 0$ . On the other hand, PV asymmetry under polarization reversal requires an integrated quantity  $\int_{-1}^1 dx \mathcal{M}_h(x)$ . These functions are divided by PE combinations of rates derived from  $\mathcal{M}_{PC1}(x), \mathcal{M}_{PC2}(x)$  in order to define normalized asymmetries. Integrated quantities are denoted by  $\tilde{\mathcal{M}}_i = \int_{-1}^1 dx \mathcal{M}_i(x)$  for subsequent use.

We do not apply external electric field to avoid possible confusion under instrumental effect [18].

### V PC rates and PV asymmetry for $^{171}\text{Yb } ^3P_2$ RENP

RENP spectral rates may be expressed by two formulas  $\Gamma_{2\nu\gamma}^\pm(\omega)$  which are interchanged by reversal of instrumental polarity; the magnetic field direction. Rates may be written as

$$\Gamma_{2\nu\gamma}^\pm(\omega) = \Gamma_{2\nu\gamma}^{PC1}(\omega) + \Gamma_{2\nu\gamma}^{PC2}(\omega) \pm \Gamma_{2\nu\gamma}^{PV}(\omega). \quad (17)$$

The last term is the interference term arising from the product of PE and PO amplitudes, while the first two terms result from the squared PE and PO amplitudes. We decompose these three spectral rates, both parity conserving (PC) and parity violating (PV), into an overall factor denoted by  $\Gamma_0$ , various spectral shape functions of kinematical nature, atomic factors, and the dynamical factor  $\eta_\omega(t)$ . We shall use a unit of 100 MHz for A-coefficients (decay rates) and eV for all energies. We give rates appropriate for Yb  $J = 2 \rightarrow 0$  RENP. The conversion factor in our natural unit is  $\hbar c = 1.97 \times 10^{-5} \text{eV} \cdot \text{cm}$ .

The overall RENP rate is given by

$$\Gamma_0 = \frac{3}{4} G_F^2 \epsilon_{eg} n^3 V \frac{\gamma_{+g}}{\epsilon_{+g}^3} \eta_\omega(t) \sim 54 \text{mHz} \left( \frac{n}{10^{21} \text{cm}^{-3}} \right)^3 \frac{V}{10^2 \text{cm}^3} \frac{\epsilon_{eg}}{\text{eV}} \frac{\gamma_{+g} \text{eV}^3}{\epsilon_{+g}^3 100 \text{MHz}} \eta_\omega(t). \quad (18)$$

The factor  $\eta_\omega(t)$  is the extractable fraction of field intensity  $\epsilon_{eg} n$  stored in the initial upper level  $|e\rangle$ . The storage and development of target polarization is induced by two trigger laser irradiation of  $\omega + \omega' = \epsilon(n'p) - \epsilon(ns), \omega < \omega'$ . The storage is due to a second order QED process, M1  $\times$  E1 type of two-photon paired super-radiance (PSR), in alkaline atoms. The calculation of  $\eta_\omega(t)$  requires numerical solution of the master equation for developing fields and target polarization given in [6], [5]. Usually,  $\eta_\omega(t)$  is much less than unity, and depends on experimental conditions.

Energy denominator factors are given by

$$\text{PE; } f_0(\omega) = \frac{\sqrt{5}b}{8(\epsilon_{eg} - \omega)} \left( \frac{c_+}{\epsilon_{+g} - \omega} + \frac{\gamma_{-g} \epsilon_{+g}^3}{\gamma_{+g} \epsilon_{-g}^3} \frac{c_-}{\epsilon_{-g} - \omega} \right), \quad (19)$$

$$c_+ = \left(1 - \frac{6a}{5b}\right) \sin \theta - 2\sqrt{2} \left(1 - \frac{8a}{5b}\right) \cos \theta, \quad (20)$$

$$c_- = \left(1 - \frac{6a}{5b}\right) \cos \theta + 2\sqrt{2} \left(1 - \frac{8a}{5b}\right) \sin \theta, \quad (21)$$

$$\text{PO; } f_1(\omega) = -\frac{1}{\epsilon_{+g} - \omega} - \frac{\gamma_{-g} \epsilon_{+g}^3}{\gamma_{+g} \epsilon_{-g}^3} \frac{1}{\epsilon_{-g} - \omega}, \quad (22)$$

with  $b, a$  two hyperfine constants, and  $\theta$  the spin-orbit mixing.

Individual contributions of remaining factors are as follows.

(1) Nuclear mono-pole PC rate assisted by hyperfine interaction is given by

$$\Gamma_{2\nu\gamma}^{PC1} = \Gamma_0 f_0^2(\omega) Q_w^2 I(\omega) \frac{3}{4} \tilde{\mathcal{M}}_{PC1}, \quad I(\omega) = 2\pi \sum_i I_{ii}(\omega) \theta(\omega_{ii} - \omega), \quad (23)$$

$$I_{ii}(\omega) = \frac{1}{2} (C_{ii}(\omega) + A_{ii}(\omega) + \delta_M m_1 m_2 D_{ii}(\omega)), \quad Q_w = N - 0.044Z. \quad (24)$$

(2) PC rate arising from squared valence spin current contribution is

$$\Gamma_{2\nu\gamma}^{PC2} = \Gamma_0 f_1^2(\omega) H(\omega; \theta_m) \frac{1}{4} \tilde{\mathcal{M}}_{PC2}, \quad H(\omega; \theta_m) = 2\pi \sum_i a_{ii}^2 H_{ii}(\omega) \theta(\omega_{ii} - \omega), \quad (25)$$

$$H_{ii}(\omega) = \frac{1}{2} (C_{ii}(\omega) - A_{ii}(\omega) - \delta_M m_i^2 D_{ii}(\omega)) + \frac{B_{ii}(\omega)}{\omega^2}. \quad (26)$$

(3) Interference term between PO and PE amplitudes is given by

$$\Gamma_{2\nu\gamma}^{PV} = -2\Gamma_0 f_0(\omega) f_1(\omega) Q_w \frac{\sqrt{3}}{4} \tilde{\mathcal{M}}_h, \quad (27)$$

$$J(\omega) = 2\pi \sum_i a_{ii} J_{ii}(\omega) \theta(\omega_{ii} - \omega), \quad J_{ii}(\omega) = -\frac{\Delta_{ii}(\omega)}{4\pi} \omega \left( \epsilon_{eg} - \frac{4}{3} \omega + \frac{4(\epsilon_{eg} - \omega) m_i^2}{3\epsilon_{eg}(\epsilon_{eg} - 2\omega)} \right). \quad (28)$$

We refer to Appendix B for  $\Delta_{ii}(\omega)$ ,  $A_{ii}(\omega)$ ,  $B_{ii}(\omega)$ ,  $C_{ii}(\omega)$ ,  $D_{ii}(\omega)$  that arise from the neutrino phase space integration. For simplicity we wrote down formulas under polarization reversal. Formulas relevant to the field reversal are obtained by replacing factors  $\tilde{\mathcal{M}}_i$  by differences at  $x = 0$  and  $x = \pi$  of corresponding functions  $\mathcal{M}_i(x)$ .

PV asymmetry is defined with appropriate choice or combinations of  $W_i$  factors as discussed in the preceding section, normalized to

$$\mathcal{A}(\omega) = \frac{2\Gamma_{2\nu\gamma}^{PV}}{\Gamma_{2\nu\gamma}^{PC1} + \Gamma_{2\nu\gamma}^{PC2}}. \quad (29)$$

This is a quantity to be compared with the experimental asymmetry obtained by taking the ratio of the difference to the sum of two rates under the field or the polarization reversal.

## VI Numerical calculation of RENP spectral rates

We numerically computed spectral rates for Yb and Xe atoms of  $^3P$  states. Below we discuss and show results of Yb, since it gives larger rates.

A-coefficients we need for computations of Yb RENP are  $\gamma_{+g} = 176, \gamma_{-g} = 1.1\text{MHz's}$  and  $\epsilon_{+g} = 3.108, \epsilon_{-g} = 2.2307, \epsilon(^3P_2) = 2.4438\text{eV's}$ . In  $^{171}\text{Yb } ^3P_2$  RENP, the dominance of the intermediate state  $^+P_1$  is evident:  $f_0(\omega) \propto -2.6/(\epsilon_{+g} - \omega) + 0.0024/(\epsilon_{-g} - \omega)$ .

Hyperfine split energies we use for  $^{171}\text{Yb}$  parameter determination (of  $b, a$ ) are [20], [21], [22],

$$\begin{aligned} \epsilon(^3P_2 5/2) - \epsilon(^3P_2 3/2) &= 6.68\text{GHz}, & \epsilon(^-P_2 3/2) - \epsilon(^-P_2 1/2) &= 5.94\text{GHz}, \\ \epsilon(^+P_2 3/2) - \epsilon(^+P_2 1/2) &= -0.32\text{GHz}. \end{aligned} \quad (30)$$

These give hyperfine parameters of  $^{171}\text{Yb } ^3P_2$ ,  $b \sim 13, a \sim 0.17\text{GHz's}$ , as discussed in Appendix D. We use these hyperfine constants and the spin-orbit mixing  $\theta$  as determined by energy levels of  $^3P_2, ^\pm P_1, ^3P_0$  in Appendix C.

PC rates and PV rate differences under field and polarization reversals are illustrated for the smallest mass of 5 meV in Fig(2)  $\sim$  Fig(4). In these figures, N Hz of rates means N number of events per second. It is difficult to distinguish the Majorana case from the Dirac case in absolute rates and PV rate differences, as seen in Fig(2) and Fig(3). But it is possible to compare Majorana-Dirac differences from PV asymmetries in lower photon energies, assuming that one can obtain a large statistics data, as seen in Fig(4). It is difficult to distinguish the Majorana neutrino pair emission from the Dirac pair emission in the examined cases.

### VII $^{171}\text{Yb } ^3P_0$ RENP

Finally, we discuss the case of  $0 \rightarrow 0$  transition. The process is of special interest, because the single photon emission is highly forbidden for this case. It turns out that PV observables are more restricted than



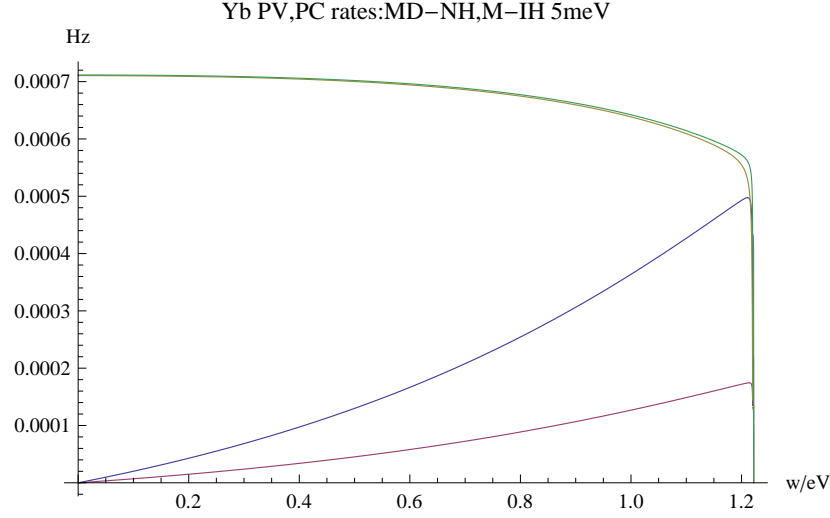


Figure 2:  $^{171}\text{Yb}$  RENP PC rates, and PV rate differences under field reversal for Majorana neutrino pair emission of smallest mass 5meV, PV-NH in blue and PV-IH in magenda, PC-NH in brown and PC-IH in green. PC rates are scaled down by 1/500 for easy comparison. Assumed parameters are target number density =  $10^{22}\text{cm}^{-3}$ , target volume =  $10^2\text{cm}^3$ .  $\eta_\omega(t) = 1$  is taken here and in all following figures.

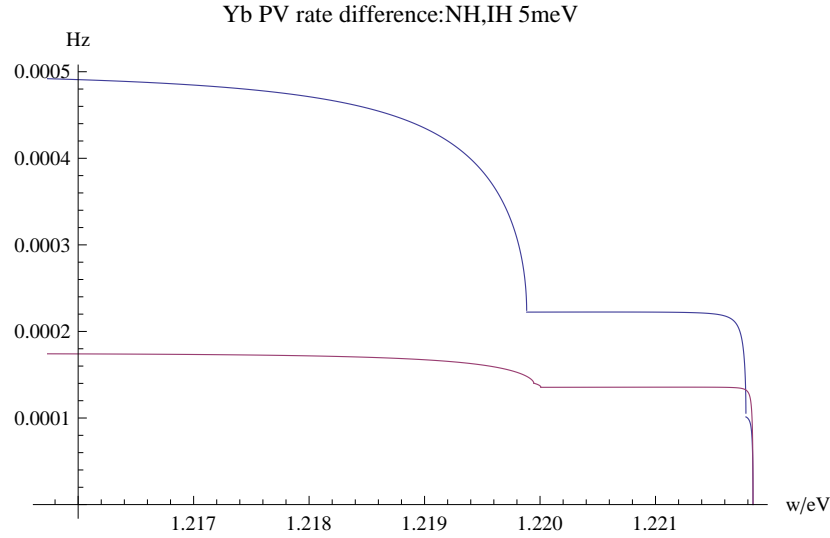


Figure 3:  $^{171}\text{Yb}$  PV rates in the threshold region corresponding to Fig(2). NH in blue and IH in magenda.

Yb PV asymmetries:MD–NH,M–IH 5meV

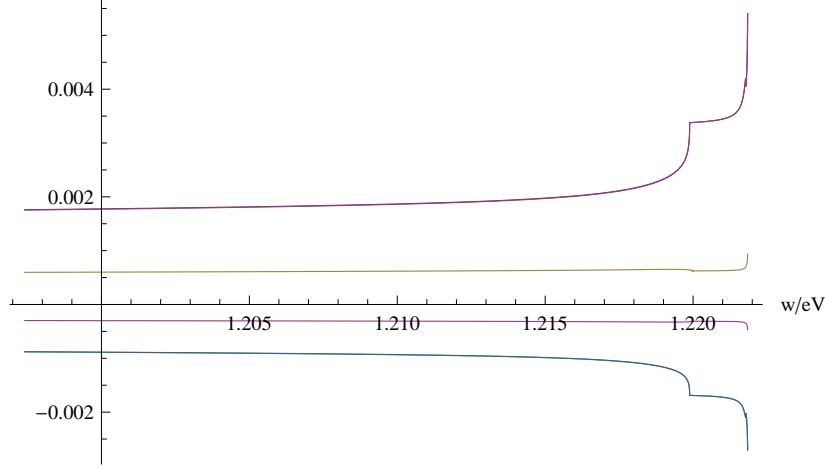


Figure 4:  $^{171}\text{Yb}$  PV asymmetries under field reversal and polarization reversal. M-NH in blue, D-NH in magenda and M-IH in brown in the positive side for field reversal, the forward-backward asymmetry. The negative value side is for PV asymmetry under polarization reversal; M-NH in green, D-NH in blue, and M-IH in magenda. MD differences are difficult to resolve with this resolution.

$^3P_2$  RENP. We describe main results briefly, since the method of computations is already explained in the  $^3P_2$  case,

Contributions from Fermi contact interaction and dipole-dipole interaction are calculated by taking explicit forms of angular parts of wave functions derived by addition of angular momenta. Results of hyperfine mixing are

$$\langle ^3P_1 F = 1/2 | \vec{I} \cdot \vec{A} | ^3P_0 F = 1/2 \rangle = -\frac{1}{2\sqrt{2}}(b - 2a), \quad (31)$$

$$\langle ^1P_1 F = 1/2 | \vec{I} \cdot \vec{A} | ^3P_0 F = 1/2 \rangle = -\frac{1}{4}(b + 2a), \quad (32)$$

$$\langle ^-P_1 F = 1/2 | \vec{I} \cdot \vec{A} | ^3P_0 F = 1/2 \rangle = -\frac{1}{2\sqrt{2}}(b - 2a) \cos \theta + \frac{1}{4}(b + 2a) \sin \theta, \quad (33)$$

$$\langle ^+P_1 F = 1/2 | \vec{I} \cdot \vec{A} | ^3P_0 F = 1/2 \rangle = -\frac{1}{4}(b + 2a) \cos \theta - \frac{1}{2\sqrt{2}}(b - 2a) \sin \theta. \quad (34)$$

Since both initial and final states have angular momentum  $J = 0$ , effects of tilted magnetic field are much simplified than the  $^3P_2$  case. PV rate differences and PC rates have the following angular dependences:

$$\text{PV}; \quad W_3^\pm(x)W_4^\pm(x) = \frac{1}{2}\sin^2 x \cos x, \quad (35)$$

$$\text{PC1}; \quad (W_3^\pm(x))^2 = \frac{1}{2}\sin^2 x, \quad (36)$$

$$\text{PC2}; \quad (W_4^\pm(x))^2 = \frac{1}{2}\sin^2 x \cos^2 x. \quad (37)$$

From these we conclude that PV asymmetry under polarization reversal given by angular integrated quantities vanish, while PV asymmetry under field reversal  $x \rightarrow \pi - x$  is non-vanishing, with

$$\text{PV asymmetry} \propto \sum_{\pm} (W_3^\pm(x)W_4^\pm(x) - W_3^\pm(\pi - x)W_4^\pm(\pi - x)) = \sin^2 x \cos x. \quad (38)$$

Note that this quantity vanishes at  $x = 0$ .

We now turn to rate formulas. The overall RENP rate is the same as in the previous  $^3P_2$  case, while energy denominator factors are given by

$$\text{PE; } f_0(\omega) = \frac{b}{4(\epsilon_{eg} - \omega)} \left( \frac{c_+^{(0)}}{\epsilon_{+g} - \omega} + \frac{\gamma_{-g}\epsilon_{+g}^3}{\gamma_{+g}\epsilon_{-g}^3} \frac{c_-^{(0)}}{\epsilon_{-g} - \omega} \right), \quad (39)$$

$$c_+^{(0)} = \sqrt{2} \left( 1 - \frac{2a}{b} \right) \sin \theta + \left( 1 + \frac{2a}{b} \right) \cos \theta, \quad (40)$$

$$c_-^{(0)} = \sqrt{2} \left( 1 - \frac{2a}{b} \right) \cos \theta - \left( 1 + \frac{2a}{b} \right) \sin \theta, \quad (41)$$

$$\text{PO; } f_1(\omega) = \sin \theta \cos \theta \left( \frac{1}{\epsilon_{+g} - \omega} + \frac{\gamma_{-g}\epsilon_{+g}^3}{\gamma_{+g}\epsilon_{-g}^3} \frac{1}{\epsilon_{-g} - \omega} \right) \quad (42)$$

We thus derive individual contributions of remaining factors in the following.

(1) Nuclear mono-pole PC rate assisted by hyperfine interaction is given by

$$\Gamma_{2\nu\gamma}^{PC1} = \Gamma_0 Q_w^2 f_0^2(\omega) I(\omega) \frac{1}{16} (W_3^\pm)^2, \quad I(\omega) = 2\pi \sum_i I_{ii}(\omega) \theta(\omega_{ii} - \omega), \quad (43)$$

$$I_{ii}(\omega) = \frac{1}{2} (C_{ii}(\omega) + A_{ii}(\omega) + \delta_M m_1 m_2 D_{ii}(\omega)), \quad Q_w = N - 0.044Z. \quad (44)$$

(2) PC rate arising from squared valence spin current contribution is

$$\Gamma_{2\nu\gamma}^{PC2} = \Gamma_0 f_1^2(\omega) H(\omega; \theta_m) \frac{2}{3} (W_4^\pm)^2, \quad H(\omega; \theta_m) = 2\pi \sum_i a_{ii}^2 H_{ii}(\omega) \theta(\omega_{ii} - \omega), \quad (45)$$

$$H_{ii}(\omega) = \frac{1}{2} (C_{ii}(\omega) - A_{ii}(\omega) - \delta_M m_i^2 D_{ii}(\omega)) + \frac{B_{ii}(\omega)}{\omega^2}. \quad (46)$$

(3) Interference term between PO and PE amplitudes is given by

$$\Gamma_{2\nu\gamma}^{PV} = -2\Gamma_0 f_0(\omega) f_1(\omega) Q_w \frac{\sqrt{2}}{4\sqrt{3}} W_1^\pm W_2^\pm, \quad (47)$$

$$J(\omega) = 2\pi \sum_i a_{ii} J_{ii}(\omega) \theta(\omega_{ii} - \omega), \quad J_{ii}(\omega) = -\frac{\Delta_{ii}(\omega)}{4\pi} \omega \left( \epsilon_{eg} - \frac{4}{3} \omega + \frac{4(\epsilon_{eg} - \omega)m_i^2}{3\epsilon_{eg}(\epsilon_{eg} - 2\omega)} \right). \quad (48)$$

Rates for  $^3P_0$  RENP are illustrated in Fig(5) by taking field reversal at  $\pi/4$  and  $3\pi/4$  angles. Rates for  $^3P_0$  RENP are typically smaller by an order of magnitudes than  $^3P_2$  RENP.

## VIII Summary

We examined how parity violating asymmetry and PV rate differences in RENP may be observed in atomic de-excitation. Large PV interference and PV asymmetry may occur in transitions among different parity states, which suggests alkaline earth atoms as good targets. We have demonstrated that large  $1/m_e$  suppression inherent in non-relativistic electrons in atoms are avoided by using the combined interference of the nuclear mono-pole and the valence spin pair emission. Fundamental formulas applicable when magnetic sub-levels are energetically resolved are derived and used for numerical computations. The PV asymmetry may reach of order a few times  $10^{-3}$  in the examined case of Yb. A further systematic search for better target atoms, especially for ions implanted in transparent crystals is indispensable for realistic RENP experiments along with extensive numerical simulations of the dynamical factor  $\eta_\omega(t)$ .

## IX Appendices

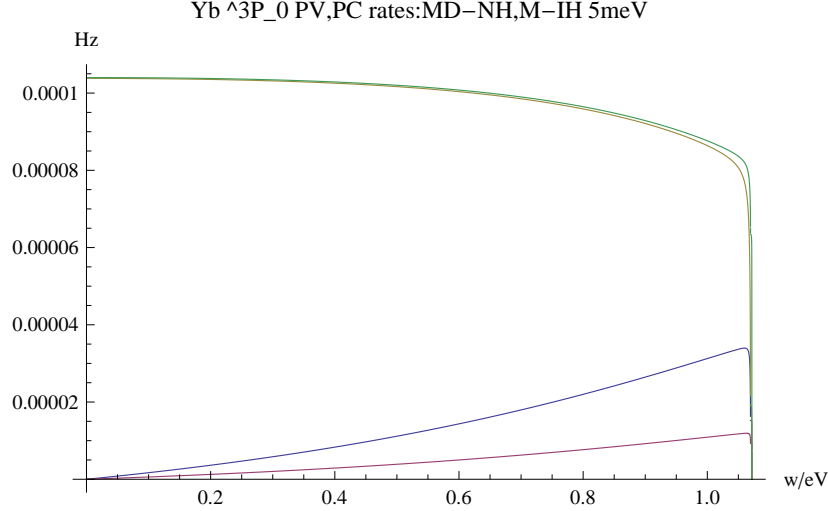


Figure 5:  $^{171}\text{Yb } ^3P_0$  RENP PC rates, and PV rate differences under field reversal for Majorana neutrino pair emission of smallest mass 5meV, PV-NH in blue and PV-IH in magenda, PC-NH in brown and PC-IH in green. PC rates are scaled down by 1/500 for easy comparison. Assumed parameters: target number density  $10^{22}\text{cm}^{-3}$ , target volume  $10^2\text{cm}^3$ .

### A: Weak hamiltonian of neutrino pair emission

We shall use the somewhat unfamiliar representation of Clifford algebra, namely the representation of diagonal  $\gamma_5 = i\gamma_0\gamma_1\gamma_2\gamma_3$  (for the purpose of the clearest distinction of Dirac and Majorana fermions). Hence it might be appropriate to clarify points that might cause confusion to the reader, which we shall explain following [4] (thereby correcting a formula there).

The basic weak hamiltonian density of neutrino pair emission that appears in atomic transitions is given by

$$\frac{G_F}{\sqrt{2}} \left( \bar{\nu}^e \gamma_\alpha (1 - \gamma_5) \nu^e \bar{\psi} \gamma^\alpha (1 - \gamma_5) \psi - \frac{1}{2} \sum_i \bar{\nu}^i \gamma_\alpha (1 - \gamma_5) \nu^i \bar{\psi} \gamma^\alpha (1 - 4 \sin^2 \theta_W - \gamma_5) \psi \right), \quad (49)$$

in the charge-retention order after Fierz transformation.

In atoms one may use expansion of the electron field operator in terms of bound state and modified plane wave functions, and we may safely ignore contribution from the plane wave part for our application. Thus we may assume that the field operator satisfies the Dirac equation; in the  $\gamma_5$ -diagonal representation,

$$\psi = \begin{pmatrix} \varphi \\ \chi \end{pmatrix}, \quad \left( E - i\vec{\sigma} \cdot \vec{\nabla} - V \right) \varphi = -m_e \chi, \quad \left( E + i\vec{\sigma} \cdot \vec{\nabla} - V \right) \chi = -m_e \varphi, \quad (50)$$

$$\left( E^2 + \vec{\nabla}^2 - 2EV - i\vec{\sigma} \cdot \vec{\nabla} V + V^2 - m_e^2 \right) \varphi = 0, \quad \chi = -\frac{1}{m_e} \left( E - i\vec{\sigma} \cdot \vec{\nabla} - V \right) \varphi. \quad (51)$$

The potential  $V$  includes the Coulomb potential and any other one-body correction to that, in the covariant  $\gamma_0 V$  form. In this  $\gamma_5$ -diagonal Majorana representation two 2-component fields  $\chi, \varphi$  are of the same order even for non-relativistic electrons.

Four vector and axial vector currents can be written in terms of two component spinors  $\varphi$  of electron

field operator as follows. Writing temporal and spatial components separately, they are

$$\begin{aligned}\bar{\psi}'\gamma_\alpha\psi &= \varphi'^\dagger \left( 1 + \frac{(E' - V + i\vec{\sigma} \cdot \vec{\nabla}')(E - V - i\vec{\sigma} \cdot \vec{\nabla})}{m_e^2} \right) \varphi, \\ -\varphi'^\dagger \left( \vec{\sigma} - \frac{(E' - V + i\vec{\sigma} \cdot \vec{\nabla}')\vec{\sigma}(E - V - i\vec{\sigma} \cdot \vec{\nabla})}{m_e^2} \right) \varphi,\end{aligned}\quad (52)$$

$$\begin{aligned}\bar{\psi}'\gamma_\alpha\gamma_5\psi &= \varphi'^\dagger \left( -1 + \frac{(E' - V + i\vec{\sigma} \cdot \vec{\nabla}')(E - V - i\vec{\sigma} \cdot \vec{\nabla})}{m_e^2} \right) \varphi, \\ \varphi'^\dagger \left( \vec{\sigma} + \frac{(E' - V + i\vec{\sigma} \cdot \vec{\nabla}')\vec{\sigma}(E - V - i\vec{\sigma} \cdot \vec{\nabla})}{m_e^2} \right) \varphi,\end{aligned}\quad (53)$$

$$\bar{\psi}'\gamma_\alpha(1 - \gamma_5)\psi = 2 \left( \varphi'^\dagger \varphi, -\varphi'^\dagger \vec{\sigma} \varphi \right), \quad (54)$$

to all orders  $1/m_e$ .  $\vec{\nabla}'$  acting on functions to the left.

To extract  $1/m_e$  terms, it is necessary to subtract the rest mass energy  $m_e$  from  $E$  and write  $E = m_e + \epsilon$ . This procedure gives

$$\mathcal{H}_W = \frac{G_F}{\sqrt{2}} \sum_{ij} j_{ij}^\alpha j_{ij,\alpha}^e, \quad j_{ij}^\alpha = \nu_i^\dagger \sigma^\alpha \nu_j, \quad (55)$$

$$j_{ij,0}^e = e^\dagger \left( b_{ij} - 2 \sin^2 \theta_W \delta_{ij} \vec{\sigma} \cdot \frac{i\vec{\nabla}}{m_e} \right) e, \quad b_{ij} = U_{ei}^* U_{ej} - \frac{\delta_{ij}}{2} (1 - 4 \sin^2 \theta_W), \quad (56)$$

$$\vec{j}_{ij}^e = e^\dagger \left( a_{ij} \vec{\sigma} + 2 \delta_{ij} \sin^2 \theta_W \frac{-i\vec{\nabla} - \vec{\sigma} \times \vec{\nabla}}{m_e} \right) e, \quad a_{ij} = -U_{ei}^* U_{ej} + \frac{1}{2} \delta_{ij}, \quad (57)$$

with  $\sigma^\alpha = (1, \vec{\sigma})$ . In writing this we changed the normalization factor of two component spinors, using the relation between 4-component and 2-component wave functions,

$$\int d^3x \bar{\psi}_n \psi_n = -2 \int d^3x \varphi_n^\dagger \left( 1 - \frac{\epsilon_n + V}{m_e} \right) \varphi_n. \quad (58)$$

Except the factor 2, there is a sign change between the two. In the non-relativistic limit,  $(\epsilon_n + V)/m_e$  term is of order  $\alpha^2$  and small.

We point out the origin of non-relativistic electron operators in Lorentz covariant currents prior to taking the non-relativistic limit: except the piece of term  $\propto a_{ij}$  all other terms come from 4-vector  $V_\alpha \propto \gamma_\alpha$ , while the term  $\propto a_{ij}$  arise from 4-axial vector  $A_\alpha \propto \gamma_\alpha \gamma_5$ . Hence PV quantities arising from electron contributions are all suppressed by  $v/c \propto 1/m_e$  effect except the interference contribution with the term  $\propto b_{ij}$  arising from core electrons. This favors heavy atoms since electron velocity in heavy atoms may be enhanced by some power of atomic number  $Z$ . The proposed PV quantity in the text is much enhanced due to a novel interference between the electron and the nuclear mono-pole current, which does not suffer from  $1/\text{mass}$  suppression at all.

## Appendix B: Neutrino phase space integral

Using the helicity summation formula of [4] and disregarding irrelevant T-odd terms, one has

$$\begin{aligned}\sum_{h_i} |j_0^\nu \cdot A_0 + \vec{j}^\nu \cdot \vec{A}|^2 &= \\ \frac{1}{2} \left( 1 + \frac{\vec{p}_1 \cdot \vec{p}_2}{E_1 E_2} + \delta_M \frac{m_1 m_2}{E_1 E_2} \right) |A_0|^2 &+ \frac{1}{2} \left( 1 - \frac{\vec{p}_1 \cdot \vec{p}_2}{E_1 E_2} - \delta_M \frac{m_1 m_2}{E_1 E_2} \right) |\vec{A}|^2 \\ &+ \frac{\Re(\vec{p}_1 \cdot \vec{A} \vec{p}_2 \cdot \vec{A}^*)}{E_1 E_2} - 2 \left( \frac{\vec{p}_1}{E_1} + \frac{\vec{p}_2}{E_2} \right) \Re(A_0 \vec{A}^*),\end{aligned}\quad (59)$$

where  $(E_i, \vec{p}_i)$  are neutrino 4-momenta. In the phase space integral of neutrino momenta,

$$\int d\mathcal{P}_\nu(\cdots) = \int \frac{d^3 p_1 d^3 p_2}{(2\pi)^2} \delta(E_1 + E_2 + \omega - \epsilon_{eg}) \delta(\vec{p}_1 + \vec{p}_2 + \vec{k})(\cdots) \quad (60)$$

one of the momentum integration is used to eliminate the delta function of the momentum conservation. The resulting energy-conservation is used to fix the relative angle factor  $\cos \theta$  between the photon and the remaining neutrino momenta,  $\vec{p}_1 \cdot \vec{k} = p_1 \omega \cos \theta$ . Noting the Jacobian factor  $E_2/p\omega$  from the variable change to the cosine angle, one obtains one dimensional integral over the neutrino energy  $E_1$ :

$$\frac{1}{2\pi\omega} \int_{E_-}^{E_+} dE_1 E_1 E_2 \frac{1}{2}(\cdots), \quad E_2 = \epsilon_{eg} - \omega - E_1. \quad (61)$$

The angle factor constraint  $|\cos \theta| \leq 1$  places a constraint on the range of neutrino energy integration,

$$E_\pm = \frac{1}{2} \left( (\epsilon_{eg} - \omega) \left( 1 + \frac{m_i^2 - m_j^2}{\epsilon_{eg}(\epsilon_{eg} - 2\omega)} \right) \pm \omega \Delta_{ij}(\omega) \right), \quad (62)$$

$$\Delta_{ij}(\omega) = \left\{ \left( 1 - \frac{(m_i + m_j)^2}{\epsilon_{eg}(\epsilon_{eg} - 2\omega)} \right) \left( 1 - \frac{(m_i - m_j)^2}{\epsilon_{eg}(\epsilon_{eg} - 2\omega)} \right) \right\}^{1/2}. \quad (63)$$

We record for completeness all four important integrals over the neutrino pair momenta:

$$\int d\mathcal{P}_\nu \frac{1}{E_1 E_2} = \frac{\Delta_{12}(\omega)}{2\pi} \equiv D(\omega), \quad (64)$$

$$\int d\mathcal{P}_\nu 1 = \frac{\Delta_{12}(\omega)}{2\pi} \left( \frac{1}{4}(\epsilon_{eg} - \omega)^2 - \frac{\omega^2}{12} + \frac{\omega^2(m_1^2 + m_2^2)}{6\epsilon_{eg}(\epsilon_{eg} - 2\omega)} - \frac{\omega^2(m_1^2 - m_2^2)^2}{12\epsilon_{eg}^2(\epsilon_{eg} - 2\omega)^2} - \frac{(\epsilon_{eg} - \omega)^2(m_1^2 - m_2^2)^2}{2\epsilon_{eg}^2(\epsilon_{eg} - 2\omega)^2} \right) \equiv C(\omega), \quad (65)$$

$$\int d\mathcal{P}_\nu \left( \frac{\vec{p}_1}{E_1} + \frac{\vec{p}_2}{E_2} \right) = -\frac{\Delta_{12}(\omega)}{4\pi} \vec{k} \left( \epsilon_{eg} - \frac{4}{3}\omega + \frac{2(\epsilon_{eg} - \omega)(m_1^2 + m_2^2)}{3\epsilon_{eg}(\epsilon_{eg} - 2\omega)} - \frac{4}{3} \frac{(\epsilon_{eg} - \omega)(m_1^2 - m_2^2)^2}{\epsilon_{eg}^2(\epsilon_{eg} - 2\omega)^2} \right) \equiv \vec{k} \frac{J(\omega)}{\omega}, \quad (66)$$

$$\int d\mathcal{P}_\nu \frac{p_1^i p_2^j + p_1^j p_2^i}{2E_1 E_2} = \frac{1}{2} (\delta_{ij} - \frac{k^i k^j}{\omega^2}) A(\omega) + \frac{1}{2\omega^2} (3 \frac{k^i k^j}{\omega^2} - \delta_{ij}) B(\omega), \quad (67)$$

$$A(\omega) = \int d\mathcal{P}_\nu \frac{\vec{p}_1 \cdot \vec{p}_2}{E_1 E_2} = \frac{\Delta_{12}(\omega)}{2\pi} \left( -\frac{1}{4}(\epsilon_{eg} - \omega)^2 + \frac{5}{12}\omega^2 + \frac{1}{2}(m_1^2 + m_2^2) + \frac{\omega^2(m_1^2 + m_2^2)}{6\epsilon_{eg}(\epsilon_{eg} - 2\omega)} - \frac{1}{12} \frac{(m_1^2 - m_2^2)^2}{\epsilon_{eg}^2(\epsilon_{eg} - 2\omega)^2} (\omega^2 + 3(\epsilon_{eg} - \omega)^2) \right) \quad (68)$$

$$B(\omega) = \int d\mathcal{P}_\nu \frac{\vec{k} \cdot \vec{p}_1 \vec{k} \cdot \vec{p}_2}{E_1 E_2} = -\frac{\Delta_{12}(\omega)}{2\pi} \frac{\omega^2}{12} (\epsilon_{eg}^2 - 2\omega\epsilon_{eg} - 2\omega^2). \quad (69)$$

### Appendix C: Intermediate coupling scheme in heavy atoms

The spin orbit interaction given by  $\sum_i^2 \xi(r_i) \vec{l}_i \cdot \vec{s}_i$  causes energy shifts and mixing of states in the  $LS$  coupling scheme. These effects becomes more important in heavier atoms. We shall derive energy eigenstates for two-electron system of  $ns, n'l$  (the angular momentua are  $0, l$ ) that includes heavy alkaline atoms. Our method is elementary and calculation is straightforward. More general method that can deal with more complicated multi-electron system is given in [15].

There are four independent states with the magnetic degeneracy of  $2J + 1$ . In the  $LS$  basis they are  $^3L_{l+1}, ^3L_l, ^1L_1, ^3L_{l-1}$  with  $L = l$ ; three spin-triplet states and one spin-singlet state. Due to the angular momentum conservation of the spin-orbit interaction the mixing occurs between  $^3L_l$  and  $^1L_l$ , and other

states become energy shifted. The  $LS$  basis we need in the following calculations are decomposition into the direct product of the spin and the orbital parts:

$$|^3P_l, l\rangle = \frac{1}{\sqrt{l+1}}(-|l, l-1\rangle_L^3|1, 1\rangle_S + \sqrt{l}|l, l\rangle_L^3|1, 0\rangle_S), \quad (70)$$

$$|^lP_l, l\rangle = |l, l\rangle_L^1|0, 0\rangle_S, \quad |^3P_{l+1}, l+1\rangle = |l, l\rangle_L^3|1, 1\rangle_S, \quad (71)$$

$$|^3P_{l-1}, l-1\rangle = \frac{1}{\sqrt{l(2l+1)}}(|l, l-2\rangle_L^3|11\rangle_S - \sqrt{2l-1}|l, l-1\rangle_L^3|1, 0\rangle_S + \sqrt{l(2l-1)}|l, l\rangle_L^3|1, -1\rangle_S), \quad (72)$$

$$|l, m\rangle_L^3 = \frac{1}{\sqrt{2}}(|l, m\rangle_1|0, 0\rangle_2 - |0, 0\rangle_1|l, m\rangle_2), \quad |l, m\rangle_L^1 = \frac{1}{\sqrt{2}}(|l, m\rangle_1|0, 0\rangle_2 + |0, 0\rangle_1|l, m\rangle_2). \quad (73)$$

We define the strength of the spin-orbit interaction in terms of the single electron matrix element,

$$\langle nljm|\xi(r)\vec{l} \cdot \vec{s}|nljm\rangle = \zeta_{nl}\frac{1}{2}\left(j(j+1) - l(l+1) - \frac{3}{4}\right). \quad (74)$$

We illustrate calculation of spin-orbit matrix elements in an example,

$$\langle ^3L_l, l|\sum_i \xi(r_i)\vec{l}_i \cdot \vec{s}_i|^1L_1, l\rangle = \langle ^3L_l, l|\sum_i \xi(r_i)\left(\frac{1}{2}(\vec{l}_{i+} \cdot \vec{s}_{i-} + \vec{l}_{i-} \cdot \vec{s}_{i+}) + \vec{l}_{iz} \cdot \vec{s}_{iz}\right)|^1L_l, l\rangle. \quad (75)$$

We note that the operation  $s_{i-}|0, 0\rangle_S \propto |1, -1\rangle_S$ , hence  $\vec{l}_{i+} \cdot \vec{s}_{i-}|^1L_l, l\rangle$  has no overlap with the initial state  $|^3L_l, l\rangle$ , as seen in formulas of the direct product decomposition. Furthermore, the operation  $s_{iz}|0, 0\rangle_S \propto |1, 0\rangle_S$  simplifies calculation. Thus, a part of the spin-orbit matrix element is calculated as

$$\langle ^3L_l, l|\xi(1)l_{1-}s_{1+}|^1L_l, l\rangle = \frac{\zeta}{\sqrt{2(l+1)}}\langle l, l-1|l_{1-}|l, l\rangle^3 = \frac{\zeta}{2}\sqrt{\frac{l}{l+1}}, \quad (76)$$

which is also equal to  $\langle ^3L_l, l|\xi(2)l_{2-}s_{2+}|^1L_l, l\rangle$ . Similarly, one has

$$\langle ^3L_l, l|\xi(1)l_{1z}s_{1z}|^1L_l, l\rangle = \frac{\zeta}{2}\sqrt{\frac{l}{l+1}}\langle l, l-1|l_{1z}|l, l\rangle^3 = \frac{\zeta}{4}l\sqrt{\frac{l}{l+1}}. \quad (77)$$

Adding all of these non-vanishing elements, one obtains

$$\langle ^3L_l, l|\sum_i \xi(r_i)\vec{l}_i \cdot \vec{s}_i|^1L_l, l\rangle = \frac{\zeta}{2}\sqrt{l(l+1)}. \quad (78)$$

Other matrix elements are calculated in similar fashions. Adding electrostatic energies and a common value for all four energy levels, the entire energy matrix is given by

$$(|^3P_2\rangle, |^3P_1\rangle, |^1P_1\rangle, |^3P_0\rangle) \begin{pmatrix} F - G + \frac{\zeta}{2}l & 0 & 0 & 0 \\ 0 & F - G - \frac{\zeta}{2} & \frac{\zeta}{2}\sqrt{l(l+1)} & 0 \\ 0 & \frac{\zeta}{2}\sqrt{l(l+1)} & F + G & 0 \\ 0 & 0 & 0 & F - G - \frac{\zeta}{2}(l+1) \end{pmatrix} \begin{pmatrix} |^3P_2\rangle \\ |^3P_1\rangle \\ |^1P_1\rangle \\ |^3P_0\rangle \end{pmatrix}. \quad (79)$$

Energy eigenvalues for the mixed  $sp$  two-electron states are, with diagonalization, given by

$$\epsilon(^3P_2) = F - G + \frac{\zeta}{2}, \quad \epsilon(^3P_0) = F - G - \zeta, \quad (80)$$

$$\epsilon_{\pm} = F - G - \frac{\zeta}{4} \pm \sqrt{(G + \frac{\zeta}{4})^2 + \frac{\zeta^2}{2}}. \quad (81)$$

Eigenstates corresponding to these energy eigenvalues are given in terms of unperturbed basis,

$$|^+P_1\rangle = \cos\theta|^1P_1\rangle + \sin\theta|^3P_1\rangle, \quad (82)$$

$$|^-P_1\rangle = \cos\theta|^3P_1\rangle - \sin\theta|^1P_1\rangle, \quad (83)$$

$$\tan(2\theta) = \frac{2\sqrt{2}\zeta}{4G + \zeta}. \quad (84)$$

There are three parameters,  $F, G, \zeta$ , in this mixing problem, and there exist four data of energies for these states. Thus, all three parameters are determined by experimental data and there is a further consistency relation (prediction) among four energies. A convenient choice is

$$\zeta = \frac{2}{3} (\epsilon(^3P_2) - \epsilon(^3P_0)), \quad (85)$$

$$F - G = \frac{1}{3} (2\epsilon(^3P_2) + \epsilon(^3P_0)), \quad (86)$$

$$F + G = \frac{1}{3} \frac{9\epsilon_+ + \epsilon_- + 4(\epsilon(^3P_2) - \epsilon(^3P_0))^2}{\epsilon(^3P_2) + 2\epsilon(^3P_0)}. \quad (87)$$

The consistency relation is given by

$$\frac{1}{2}(\epsilon_+ + \epsilon_-) = \frac{1}{6}(\epsilon(^3P_2) + 2\epsilon(^3P_0)) + \frac{1}{6} \frac{9\epsilon_+ + \epsilon_- + 4(\epsilon(^3P_2) - \epsilon(^3P_0))^2}{\epsilon(^3P_2) + 2\epsilon(^3P_0)} \quad (88)$$

The mixing angle  $\theta$  calculated from experimental data of Yb  $6s6p$ -system is  $\sim 0.16$ . Accuracy of the consistency relation (88) is something like 2.669 (LHS) vs 2.676(RHS) and is excellent.

Following [15], one may use a convenient set of parameters for the energy level diagram;

$$\eta = \frac{\epsilon}{G\sqrt{1+\chi^2}}, \quad \frac{\chi}{1+\chi}, \quad (89)$$

with  $\chi \equiv 3\zeta/(4G)$ , for the energy and for the strength of  $LS$ -interaction, respectively. In the weak coupling limit  $\eta_{\pm} \rightarrow \pm 1$  as  $\chi \rightarrow 0$ , and  $\eta_{\pm} \rightarrow 2/3, -4/3$  as  $\chi \rightarrow \infty$ .

The energy curves are plotted in Fig(6). These curves are universal for all alkaline earth atoms. Three sets of atomic data of Sr, Yb, and Hg and Xe of electron-hole system of the same quantum numbers as alkaline earth atoms are compared with these curves: the agreement of theoretical curves and data are good.

## Appendix D: Hyperfine interaction

Nucleus may produce various types of multi-pole fields. Most important are magnetic field by their magnetic dipole moment and electric quadrupole field by nuclear quadrupole moment.

Magnetic hyperfine interaction arises from interaction of electron magnetic dipole moment with the nuclear magnetic field. The interaction may be written in the product form of electron and nuclear magnetic moments, or their angular momenta. A standard hyperfine interaction for a single electron is [16]

$$\mathcal{H}_h = g_e g_N \mu_B \mu_N \left( \frac{\vec{I} \cdot (\vec{L} - \vec{S})}{r^3} + \frac{3\vec{I} \cdot \vec{r} \vec{S} \cdot \vec{r}}{r^5} + \frac{8\pi}{3} \delta(\vec{r}) \vec{I} \cdot \vec{S} \right), \quad (90)$$

where  $\vec{S}, \vec{L}$  are electron spin and orbital angular momentum operator and  $\vec{I}$  is the nuclear spin operator. The first two terms are the dipole-dipole interaction restricted to atomic orbitals of non-vanishing angular momentum. while the third is the Fermi contact interaction restricted to s-orbitals of non-vanishing wave functions at the origin of nucleus.



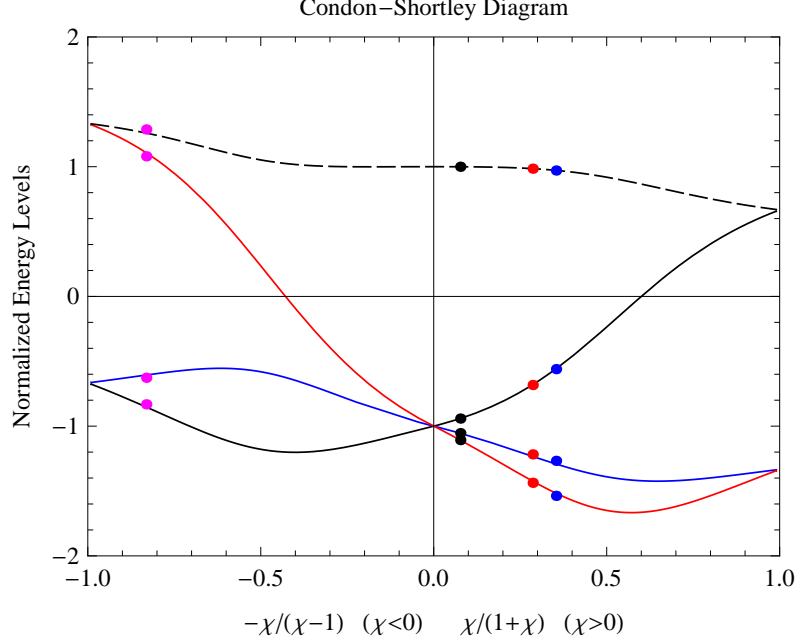


Figure 6: Condon-Shortley diagram for alkali earth atoms: the variable  $\eta$  plotted against  $\chi/(\chi + 1)$  of eq.(89). Experimental data of level energies of  $^+P_1, ^3P_2, ^-P_1, ^3P_0$  (from the upper to the lower) of Sr, Yb, and Hg are plotted in dots; from the left to the right in the right  $\chi > 0$ . Xe data of  $\chi < 0$  are in the left.

We have in mind applications in RENP, and use of atoms with two-electron system of two kinds; alkaline earth like atoms made of  $ns, n'p$ . Transition to intermediate state in RENP occurs by hyperfine interaction bridging different  $J$  states of two-electron,  $^3P_2 \rightarrow ^\pm P_1$  in alkaline earth atoms of odd isotopes such as  $^{171}\text{Yb}$ .

For simplicity we consider a specific transition from the state of  $F = M_F = 3/2$ . Using the Wigner-Eckart theorem [17], one can separate the nuclear part and the atomic part as [16]

$$\langle ^\pm P_1 I J F | \vec{I} \cdot \vec{A} | ^3 P_2 I J' F \rangle = (-1)^{F+J'+I} \left\{ \begin{matrix} I & J' & F \\ J & I & 1 \end{matrix} \right\} \langle ^\pm P_1 I || \vec{I} || ^\pm P_1 I \rangle \langle ^\pm P_1 || \vec{A} || ^3 P_2 \rangle, \quad (91)$$

with the 6j symbol here

$$\left\{ \begin{matrix} 1/2 & J' & 3/2 \\ J & 1/2 & 1 \end{matrix} \right\}, \quad (92)$$

readily available for  $(J', J) = (2, 1)$ . Reduced matrix elements  $\langle ^\pm P_1 || \vec{A} || ^3 P_2 \rangle$  are calculated using wave functions of two-electron system. Final results may be expressed in terms of matrix elements of single electron states;

$$a = g_e g_N \mu_B \mu_N \langle 6p | \frac{1}{r^3} | 6p \rangle, \quad b = g_e g_N \mu_B \mu_N \frac{8\pi}{3} |\psi_{6s}(0)|^2. \quad (93)$$

In order to determine parameters  $a, b$  of hyperfine interaction, we calculate hyperfine split levels. Splitting follows the rule for different  $F$ ;  $A(F(F+1) - J(J+1) - I(I+1))/2$  even under the presence of dipole-

dipole interaction [16]. Diagonal matrix elements we need are calculated as

$$\langle {}^3P_2 5/2 | \vec{I} \cdot \vec{A} | {}^3P_2 5/2 \rangle = \frac{1}{2\sqrt{6}}(b + \frac{14}{5}a), \quad (94)$$

$$\langle {}^3P_1 3/2 | \vec{I} \cdot \vec{A} | {}^3P_1 3/2 \rangle = \frac{1}{8}(b + 10a), \quad (95)$$

$$\langle {}^1P_1 3/2 | \vec{I} \cdot \vec{A} | {}^1P_1 3/2 \rangle = \frac{1}{2}a. \quad (96)$$

Taking into account of the spin-orbit interaction, the magnitudes of splitting are then given by

$$\epsilon({}^3P_2, F = 5/2) - \epsilon({}^3P_2, F = 3/2) = \frac{5}{4\sqrt{6}}(b + \frac{14}{5}a), \quad (97)$$

$$\epsilon({}^-P_1, F = 3/2) - \epsilon({}^-P_1, F = 1/2) = \frac{3}{8}(b + 10a) \cos^2 \theta - \frac{3}{2\sqrt{2}}(b + \frac{13}{5}a) \sin \theta \cos \theta + \frac{3}{2}a \sin^2 \theta, \quad (98)$$

$$\epsilon({}^+P_1, F = 3/2) - \epsilon({}^+P_1, F = 1/2) = \frac{3}{2}a \cos^2 \theta + \frac{3}{2\sqrt{2}}(b + \frac{13}{5}a) \sin \theta \cos \theta + \frac{3}{8}(b + 10a) \sin^2 \theta. \quad (99)$$

No splitting exists for  $\epsilon({}^3P_0, F = 1/2)$ . Without the spin-orbit interaction  $\theta = 0$  and  ${}^+P_1$  hyperfine splitting is purely given by dipole-dipole interaction  $\propto a$ .

From experimental data we may determine  $b \sim 12.6\text{GHz}$ ,  $a \sim 0.17\text{GHz}$  and  $\theta \sim -0.04$ . The agreement of the spin-orbit mixing  $\theta$  with the analysis in the preceding Appendix C is not good. The contribution of dipole-dipole interaction is however much smaller  $a/b \sim 1/70$  than the Fermi contact term, and it would be sufficient to neglect the dipole-dipole interaction in hyperfine splitting. Moreover, the estimate of the spin-orbit mixing  $\theta$  in the preceding section appears more reliable.

Hyperfine interaction causes mixing of states defined in the intermediate coupling such as  ${}^3P_2$  and  $\pm P_1$ . Magnitudes of this coupling are given in the text.

## Appendix E: Magnetic factors and angular distributions

One needs to consider two amplitudes, parity even (PE) and parity odd (PO), in order to induce PV effects. PE amplitude consists of hyperfine interaction sandwiched in time sequence between the nuclear mono-pole neutrino pair emission and E1 photon emission from the valence line. PO amplitude consists of M1 type pair emission followed by E1 photon emission.

We apply a magnetic field directed by an angle  $\theta_m$  away from the propagation (also the trigger axis). All states are classified by specifying the magnetic quantum numbers along the magnetic field. We assume that at least electronic states are energetically resolved by the magnetic field.

Disregarding energy denominators and coupling factors, PE matrix elements are given in the  $\vec{F}$ -basis ( $\vec{F} = \vec{J} + \vec{I}$  is the total angular momentum of atoms and nucleus) by

$$-\sqrt{3} \sum_{F,M} d_{M'_F, M}^F d_{M_F, M \pm 1}^{1/2} (-1)^{1/2 - M \mp 1} \begin{pmatrix} 1/2 & 1 & F \\ -M \mp 1 & \pm 1 & M \end{pmatrix} \quad (100)$$

$$\cdot \langle {}^{3,1}P_1 F = 3/2, M'_F | \vec{I} \cdot \vec{A} | {}^3P_2 F = 3/2, M'_F \rangle. \quad (101)$$

We may define the magnetic factor for PE amplitude disregarding the angle independent factor of eq.(101) and calculate ( $\pm$  corresponding to circular polarizations of  $\pm 1$ )

$$\begin{aligned} & \sum_{F,M} d_{M'_F, M}^F d_{M_F, M \pm 1}^{1/2} (-1)^{1/2 - M \mp 1} \begin{pmatrix} 1/2 & 1 & F \\ -M \mp 1 & \pm 1 & M \end{pmatrix} \\ &= \frac{1}{2\sqrt{3}}(d_{M'_F, -1/2}^{3/2} d_{M_F, 1/2}^{1/2} + \sqrt{3} d_{M'_F, -3/2}^{3/2} d_{M_F, -1/2}^{1/2}) = \frac{1}{2} d_{1,-1}^1, \quad \text{for } h = 1 \end{aligned} \quad (102)$$

$$= \frac{1}{2\sqrt{3}}(d_{M'_F, 1/2}^{3/2} d_{M_F, -1/2}^{1/2} + \sqrt{3} d_{M'_F, 3/2}^{3/2} d_{M_F, 1/2}^{1/2}) = \frac{1}{2} d_{1,1}^1, \quad \text{for } h = -1 \quad (103)$$

The equality of d-functions is as expected since one can equally work out the magnetic factor without the nuclear spin in this case.

The PO amplitude has matrix element product in the  $\vec{J}$ -basis,

$$\begin{aligned} & \langle {}^1S_0 | Y_{1,\pm 1} S_z | {}^3P_2, \tilde{M}_J' \rangle \\ &= \frac{1}{\sqrt{30}} \langle {}^1S_0 || \vec{Y} || {}^\pm P_1 \rangle \langle {}^\pm P_1 || \vec{S} || {}^3P_2 \rangle \sum_M d_{M,\mp 1}^1 (-d_{M',1}^2 d_{M,1}^1 + \frac{2}{\sqrt{3}} d_{M',0}^2 d_{M,0}^1 - d_{M',-1}^2 d_{M,-1}^1), \end{aligned} \quad (104)$$

$$\langle {}^+P_1 || \vec{S} || {}^3P_2 \rangle = \sqrt{\frac{5}{2}} \sin \theta, \quad \langle {}^-P_1 || \vec{S} || {}^3P_2 \rangle = \sqrt{\frac{5}{2}} \cos \theta, \quad \langle {}^1S_0 || \vec{Y} || {}^\pm P_1 \rangle = -\sqrt{3}. \quad (105)$$

In order to define magnetic factors, we introduce

$$\begin{aligned} W_2^\pm(x) &= \sum_M d_{M,\pm 1}^1(x) \left( -\sqrt{3} d_{1,1}^2(x) d_{M,1}^1(x) + 2 d_{1,0}^2(x) d_{M,0}^1(x) - \sqrt{3} d_{1,-1}^2(x) d_{M,-1}^1(x) \right) \\ W_2^+(x) &= \frac{\sqrt{3}}{2} (-\cos x + \cos(2x)), \quad W_2^-(x) = \frac{\sqrt{3}}{2} (-\cos x - \cos(2x)), \end{aligned} \quad (106)$$

$$W_1^+(x) = d_{1,-1}^1(x) = \sin^2 \frac{x}{2}, \quad W_1^-(x) = d_{1,1}^1(x) = \cos^2 \frac{x}{2}. \quad (107)$$

Explicit functional forms have been calculated using Mathematica.

Adding two circular polarizations gives the angular distribution from a polarized atom, for instance from  $J = 2, M_J = 1$  in the example above. These are given by elementary functions:

PV quantity

$$W_1^+ W_2^+ + W_1^- W_2^- = -\sqrt{3} \cos^3 x. \quad (108)$$

PC quantities

$$(1) (W_1^+)^2 + (W_1^-)^2 = \frac{1}{4} (3 + \cos(2x)), \quad (109)$$

$$(2) (W_2^+)^2 + (W_2^-)^2 = \frac{3}{4} (2 + \cos(2x) + \cos(4x)). \quad (110)$$

These functions satisfy the obvious constraint under the transformation,  $x \rightarrow \pi - x$ . PC quantities must be even under this transformation, while PV quantity may contain odd piece.

In Fig(7) the magnetic field directional dependence as given by the formulas above is illustrated for the transition  $F = 3/2, M_F = 3/2 \rightarrow F = 1/2, M_F = 1/2$ . Two contributions of different circular polarizations are added.

**Acknowledgements** We should like to thank T. Wakabayashi for a valuable discussion. This research was partially supported by Grant-in-Aid for Scientific Research on Innovative Areas "Extreme quantum world opened up by atoms" (21104002) from the Ministry of Education, Culture, Sports, Science, and Technology.

## References

- [1] G. L. Fogli, E. Lisi, A. Marrone, D. Montanino, A. Palazzo, and A. M. Rotunno, *Phys. Rev. D* **86**, 013012 (2012) [10 pages].
- M. C. Gonzalez-Garcia, Michele Maltoni, Jordi Salvado, Thomas Schwetz, *Journal of High Energy Physics* **December 2012**, 123.
- D. V. Forero, M. Toacutertola, and J. W. F. Valle, *Phys. Rev. D* **86**, 073012 (2012) [8 pages].

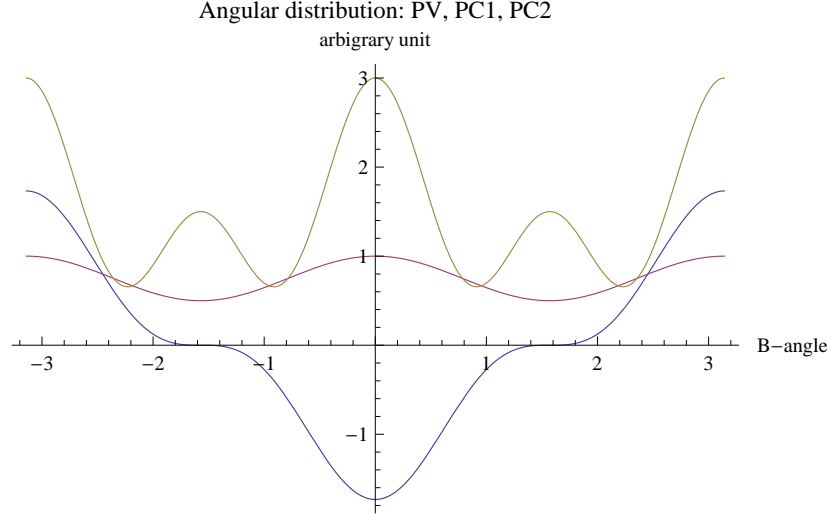


Figure 7: Angular distributions for PV rate difference in blue, two PC rates in magenda and brown, the angle measured from the magnetic field direction for  $^3P_2 M_J = 3/2 \rightarrow ^1S_0 1/2$

- [2] G. Drexlin, V. Hannen, S. Mertens, and C. Weinheimer, *Current Direct Neutrino Mass Experiments*, Advances in High Energy Physics Volume 2013 (2013)Article ID 293986.
- [3] A. Gando et al, *Phys. Rev. Lett.***110**, 062502 (2013), and arXiv:1201.4664v2[hep-ex] (2012).  
M.Auger et al, *Phys. Rev. Lett.***109**, 032505 (2012).
- [4] M. Yoshimura, *Phys. Rev.***D75**. 113007 (2007).
- [5] A. Fukumi et al., *Progr. Theor. Exp. Phys.***2012**, **04D002**; arXiv1211.4904v1[hep-ph](2012).
- [6] M. Yoshimura, N. Sasao, and M. Tanaka, *Phys. Rev* **A86**,013812(2012), and *Dynamics of paired super-radiance*, arXiv:1203.5394[quan-ph] (2012).
- [7] M. Yoshimura, *Phys. Lett.***B699**,123(2011).  
D.N. Dinh, S. Petcov, N. Sasao, M. Tanaka, *Phys. Lett.***B719**,154(2012), and arXiv1209.4808v1[hep-ph].
- [8] M. Yoshimura and N. Sasao, *Radiative emission of neutrino pair from nucleus and inner core electrons in heavy atoms*, arXiv:1310.6472v1 [hep-ph](2013).
- [9] M.A. Bouchiat and C. Bouchiat, *J. Phys. (Paris)***35**, 899 (1974); *ibid.* **36**,493 (1975).
- [10] M.A. Bouchiat et al, *Phys. Lett.***134B**, 463(1984), and references therein.
- [11] P.S. Drell and E.D. Commins, *Phys. Rev.***A 32**, 2196(1985), and references therein.
- [12] M.C. Noecker, B.P. Materson, and C.E. Wieman, *Phys. Rev. Lett.***61**, 310 (1988), and references therein.
- [13] J. Alnis, A. Matveev, N. Kolachevsky, T. Udem, and T. W. Hänsch, *Phys. Rev.* **A77**, 053809 (2008).
- [14] B.H. Bransden and C.J. Joachain, *Physics of Atoms and Molecules*, 2nd edition, Prentice Hall(2003).
- [15] E.U. Condon and G.H. Shortley, *The Theory of Atomic Spectra*, Cambridge University Press (1951).

- [16] M. Weissbluth, *Atoms and Molecules*, Academic Press (1978). We follow the sign and normalization conventions of this book in our calculations of hyperfine interaction.
- [17] M.E. Rose, *Elementary Theory of Angular Momentum*, Dover (1957).
- [18] Results of the following paper by some of us, M. Yoshimura, A. Fukumi, N. Sasao, and T. Yamaguchi *Progr. Theor. Phys.***123**,523(2010), contain effects linear in the applied static Stark field, hence the main part of its results reflects the instrumental PV asymmetry rather than the intrinsic PV asymmetry of fundamental theory.
- [19] In [5] a result for numerical simulation of  $\eta_\omega(t)$  is presented for  $\text{pH}_2$  molecule target (strong source of paired super-radiance (PSR) of  $E1 \times E1$  transition, and see Fig 14 of this reference for time dependence). Its time dependence is complicated: a fast rise in  $O(2 \text{ ns})$ , then a plateau region of magnitude  $O(10^{-2} \sim 10^{-3})$  of duration of several nano-seconds, finally gradual decrease ending around  $10^{-6}$  at  $\sim 12 \text{ ns}$  (end time of calculation). For RENP rate calculations, numerical simulations based on the master equation given in [5] should be performed for weaker PSR process of specific targets considered, which is expected to give different time profile and larger values of  $\eta_\omega(t)$ .
- [20] T. Wakui, W.-G. Jin, K. Hasegawa, H. Uematsu, T. Minowa, and H. Katsuragawa, *J. Phys. Soc. Jpn.***72**, 2219 (2003).
- [21] D. L. Clark, M. E. Cage, D. A. Lewis, and G. W. Greenlees, *Phys. Rev.* **A20**, 239 (1979).
- [22] D. Das, S. Barthwal, A. Banerjee, and V. Natarajan, *Phys. Rev.* **A72**, 032506 (2005).